Nongray Radiating Flow about Smooth Symmetric Bodies

W. B. OLSTAD*
NASA Langley Research Center, Hampton, Va.

A simplified flowfield technique developed by S. H. Maslen was modified to account for radiation and large blowing. Radiation cooling and nongray absorption (including the contribution of atomic lines) were taken into account. Results were obtained for a series of blunted cones traveling at speeds from 10.7 to 15.2 km/sec at an altitude of 60.96 km in the Earth atmosphere. It is shown that the radiative heating distributions depend strongly on whether the primary source of radiation is the entropy layer or the flow external to the entropy layer. It is also shown that the entropy layer can be significantly affected by radiation cooling. The reduction of radiative heating by blowing cold air from the body surface is also discussed.

Nomenclature

A = constant in Eq. (23)
B_i = partial integral of the Planck function
$\bar{B}_{\bar{\nu}}$ = Planck function at frequency $\bar{\nu}$
C_{HR} = heat-transfer coefficient for radiation, $\bar{q}_w{}^R/\frac{1}{2}\bar{\rho}_\infty \bar{V}_\infty{}^3$
(e^-) = number density of free electrons
f_1, f_2 = functions defined by Eqs. (A22) and (A25), respectively
h = nondimensional enthalpy, $h/\frac{1}{2}V_\infty{}^2$
$\bar{h}$ = enthalpy
h_{eff} = nondimensional effective heat of ablation, $\bar{h}_{\text{eff}}/\frac{1}{2}\bar{V}_\infty{}^2$
$\bar{h}_{\text{eff}}$ = effective heat of ablation
$\bar{h}^*$ = reference enthalpy defined by Eq. (A20)
j = 0 or 1 for plane or axisymmetric flow
k_p = Bouguer number, $\bar{\rho}_\infty \bar{\kappa}_{p,st} \bar{R}_{st}$
K_s = nondimensional shock curvature, $\bar{R}_{st}\bar{K}_s$
$\bar{K}_s$ = shock curvature
(N) = number density of nitrogen atoms
(N_2) = number density of nitrogen molecules
(O) = number density of oxygen atoms
(O_2) = number density of oxygen molecules
p = nondimensional pressure, $\bar{p}/\bar{\rho}_\infty \bar{V}_\infty{}^2$
$\bar{p}$ = pressure
$q_w{}^R$ = nondimensional radiative heat flux at the body surface $\bar{q}_w{}^R/\frac{1}{2}\bar{\rho}_\infty \bar{V}_\infty{}^3$
$\bar{q}_w{}^R$ = radiative heat flux at the body surface
$q_\psi{}^R$ = nondimensional ψ component of the radiative heat-flux vector, $\bar{q}_\psi{}^R/\frac{1}{2}\bar{\rho}_\infty \bar{V}_\infty{}^3$
$\bar{q}_\psi{}^R$ = ψ component of the radiative heat-flux vector
Q = function defined by Eq. (16)
Q_{bl} = function defined by Eq. (22)
Q_{sl} = function defined by Eq. (21)
r = nondimensional radial coordinate, $4\bar{r}/\bar{R}_b$
$\bar{r}$ = radial coordinate
$\bar{R}_b$ = base radius of the body
$\bar{R}_{st}$ = radius of curvature of shock at the stagnation streamline
T = nondimensional temperature, $\bar{T}/\bar{T}_{st}$
$\bar{T}$ = temperature
$\bar{T}_{st}$ = temperature immediately behind the shock on the stagnation streamline
$\tilde{T}$ = nondimensional temperature defined by Eq. (A9)
u = nondimensional tangential velocity component, $\bar{u}/\bar{V}_\infty$
$\bar{V}_\infty$ = freestream velocity
x = nondimensional coordinate measured along the shock, $4\bar{x}/\bar{R}_b$
$\bar{x}$ = coordinate measured along the shock
y = nondimensional coordinate measured normal to the shock, $4\bar{y}/\bar{R}_b$
$\bar{y}$ = coordinate measured normal to the shock
z = nondimensional axial coordinate, $4\bar{z}/\bar{R}_b$
$\bar{z}$ = axial coordinate
Δ_{bL} = nondimensional local blown-layer thickness defined by Eq. (13)
Δr = increment of r
ϵ = radiation cooling parameter, $(4\sigma \bar{T}_{st}{}^4/\bar{\rho}_\infty \bar{V}_\infty{}^3)k_p$
ζ_1, ζ_2 = functions defined by Eqs. (A23) and (A26), respectively
θ_s = half angle of cone which is shock shape asymptote for large r_s
κ_i = nondimensional mass absorption coefficient for step i, $\bar{\kappa}_i/\bar{\kappa}_{p,st}$
$\bar{\kappa}_i$ = mass absorption coefficient for step i
$\bar{\kappa}_{p,st}$ = Planck mean mass absorption coefficient evaluated immediately behind the shock on the stagnation streamline
λ = wavelength
$\bar{\mu}_{\bar{\nu}}$ = linear monochromatic absorption coefficient
$\bar{\nu}$ = nondimensional frequency defined by eq. (A10)
ξ = dummy variable of integration
ρ = nondimensional density, $\chi\bar{\rho}/\bar{\rho}_\infty$
$\bar{\rho}$ = density
σ = Stefan-Boltzmann constant
τ_i = normalized optical depth for step i defined by Eq. (17)
χ = ratio of freestream density to density immediately behind the shock on the stagnation streamline
ψ = nondimensional stream function, $\psi/\bar{\rho}_\infty \bar{V}_\infty \bar{R}_{st}{}^{j+1}$
$\bar{\psi}$ = stream function

Subscripts

s = conditions immediately behind the shock wave
st = conditions immediately behind the shock wave on the stagnation streamline
w = body surface conditions
0 = sea-level reference conditions
∞ = freestream

Superscript

(k) = kth iterate

Introduction

A NUMBER of studies are available which treat the flow of an equilibrium radiating gas in the stagnation region of a blunt body.[1-4] All of the studies cited include the effects of radiation cooling and nongray absorption and use realistic models for the absorption coefficient of high-temperature air, which include the contribution of atomic lines. Some studies[3,5,6] have included ablation effects as well.

While much is now known about the behavior of equilibrium, radiating gases in stagnation region flows, much remains to be learned about the behavior of these gases downstream of the stagnation point. Cheng and Vincenti[7] considered the effect of radiation in the subsonic region behind a paraboloidal shock wave. Wang[8] considered the flows over a sharp wedge, a sharp cone, and the subsonic portion of a sphere. Both studies assumed that the gas was gray. Hoshizaki and Wilson[9] and Suttles[10] included nongray effects,

Presented as Paper 69-637 at the AIAA 4th Thermophysics Conference, San Francisco, Calif., June 16-18, 1969; submitted October 13, 1969; revision received June 22, 1970. The author gratefully acknowledges the assistance of J. T. Kemper who programed the equations for machine computations.

* Head, Gas Physics Section. Member AIAA.

although the first authors neglected the atomic line contribution in their studies of the subsonic flow region about a sphere. Recently Burns and Oliver[11] presented some results of radiative heating calculations for a wide-angle conical body. Their calculations were performed for a transparent (emitting but nonabsorbing) gas, although they did draw some conclusions about the effect of self-absorption for a two-step (in frequency) model absorption coefficient.

The present work was undertaken to study the equilibrium, radiating flow about smooth symmetric bodies. The effects of radiation cooling and nongray absorption are included. An absorption coefficient model similar to that used in Refs. 1 and 2, which includes the contribution of atomic lines, is used herein. The flowfield is computed with a method developed by Maslen[12] modified to account for radiation. Thus the present approach is inverse (the shock geometry rather than the body geometry is specified initially) and not strictly valid in the stagnation region. The boundary conditions on the body surface have been written to allow for an inviscid blown layer with the blowing rate related to the net radiative heating rate through an effective heat of ablation. When the nondimensional blowing rate is large compared to the inverse square root of the local Reynolds number, viscous effects will be confined to a thin shear layer in the vicinity of the dividing streamline between the shock and blown layers.[13] This will be the case when the radiative heating rates are large so that there is some justification for treating the blown layer as inviscid. However, even when such a treatment is not justified on the grounds previously discussed, the inviscid analysis does provide a means for studying the effects of absorption by a cold layer of one nongray gas on the radiative heat flux issuing from a hot layer of another nongray gas.

Results are presented for a series of blunted cones in air, without blowing, for a range of bluntness parameter and cone angle. In addition, results are presented for a paraboloidal shock, including the effects of blowing for a range of effective heats of ablation. The blown gas is assumed to have the same properties as air.

Analysis

The shock layer formed about a smooth, symmetric body at hypersonic speeds is quite thin. Furthermore, at some not too large distance downstream of the stagnation point the flow direction in the shock layer is nearly parallel to the shock. S. H. Maslen[12] took advantage of this situation to derive a simplified system of equations which adequately describe the flow and thermodynamic properties in the shock layer for an inviscid, nonreacting, nonradiating gas for a given shock shape. The most important step in the derivation was the transformation to the von Mises plane and the subsequent uncoupling of the y momentum equation [the y direction is normal to the shock in the shock-oriented coordinate system (Fig. 1)] from the other equations. This led to an expression for the pressure which depends only on the shock geometry and the stream-function coordinates. In nondimensional form this expression is

$$p(x,\psi) = p_s(x) + [K_s(x)u_s(x)/r_s{}^j(x)][\psi - \psi_s(x)] \quad (1)$$

The addition of a radiant energy transport term (the divergence of the radiation flux vector) to the energy equation does not alter this result. The two remaining equations, the x momentum equation (the x direction is parallel to the shock) and the energy equation, when simplified in the manner prescribed by Maslen, are

$$u(\partial u/\partial x) + (\chi/\rho)(\partial p/\partial x) = 0 \quad (2)$$

$$\partial h/\partial x + u(\partial u/\partial x) = r_s{}^j \partial R_\psi{}^R/\partial\psi \quad (3)$$

Here j is zero for two-dimensional flow and one for axisymmetric flow, χ is the ratio of freestream to shocked gas density across a normal shock traveling at the same speed and in the same ambient conditions as the body, and $\partial_{q\psi}{}^R/\partial\psi$ is the nondimensional divergence of the radiation flux vector (the x component of the radiation flux vector has been neglected as a result of the thin shock-layer approximation). For the purposes of this paper, the gas is assumed to obey the simplified equation of state.

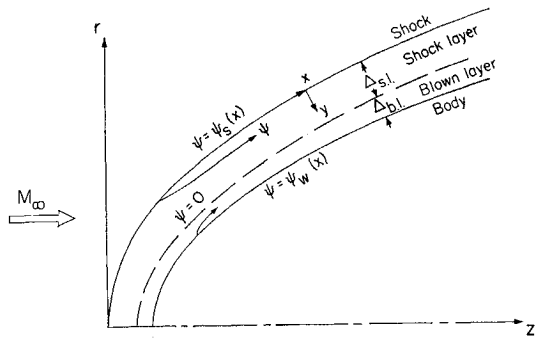

Fig. 1 Geometry of the flow.

$$h = (1 + \chi)p/\rho \quad (4)$$

Because local thermodynamic equilibrium is assumed, the divergence of the radiation flux vector can be expressed as a function of the thermodynamic properties (in this case p and ρ) and the geometry of the shock layer. Combining Eqs. (2–4) leads to an integrodifferential equation for the nondimensional density ρ

$$(\partial\rho/\partial x) - [(1 - \chi)/(1 + \chi)](\partial p/p\partial x)\rho = [r_s{}^j\rho^2/(1 + \chi)p](\partial q_\psi{}^R/\partial_\psi) \quad (5)$$

The appropriate boundary condition is

$$\rho = \rho_s(\psi), \text{ at } x = x_s(\psi) \quad (6)$$

The subscript s refers to conditions immediately behind the shock. Once the density has been obtained, the velocity u can be determined by integration of Eq. (2) and application of the boundary condition

$$u = u_s(\psi), \text{ at } x = x_s(\psi) \quad (7)$$

The result is

$$u(x,\psi) = \left[u_s{}^2(\psi) - 2\chi\int_{x_s(\psi)}^{x} \frac{1}{\rho}\frac{\partial p}{\partial x}\,dx\right]^{1/2} \quad (8)$$

For no blowing, the body is located at the surface where the stream function ψ is zero and the shock layer standoff distance is given by the integral

$$\Delta_{sl}(x) = \frac{\chi}{r_s{}^j(x)}\int_0^{\psi_s(x)} \frac{d\psi}{\rho u} \quad (9)$$

With blowing Eq. (9) locates the shock-layer blown-layer interface. The density in the blown layer is determined by solving Eq. (5) with the boundary condition

$$\rho = \rho_w(x), \text{ at } x = x_w(\psi) \quad (10)$$

and the blown-layer velocity distribution is obtained by integrating Eq. (2) with the condition

$$u = 0, \text{ at } x = x_w(\psi) \quad (11)$$

This gives

$$u(x,\psi) = \left[-2\chi\int_{x_w(\psi)}^{x} \frac{1}{\rho}\frac{\partial p}{\partial x}\,dx\right]^{1/2} \quad (12)$$

It is evident from Eq. (12) that a favorable pressure gradient is necessary to drive the flow in the blown layer. The

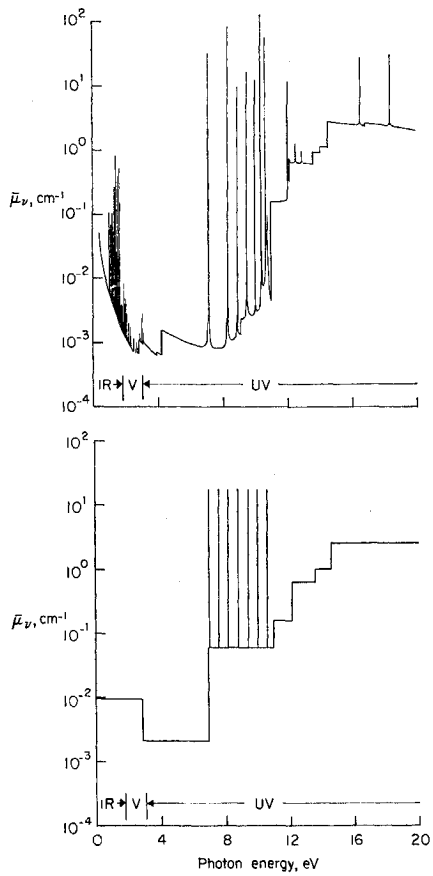

Fig. 2 Detailed and step model absorption coefficients for air; $\bar{T} = 14000°\text{K}$, $\bar{\rho}/\bar{\rho}_0 = 10^{-2}$.

same requirement was noted by Cole and Aroesty in their study of the Blowhard Problem.[13]

The thickness of the blown layer is given by the integral

$$\Delta_{bl}(x) = \frac{\chi}{r_s{}^j(x)} \int_{\psi_w(x)}^{0} \frac{d\psi}{\rho u} \tag{13}$$

Values of the nondimensional stream function at the shock and at the body surface with blowing are given by the formulas

$$\psi_s(x) = [r_s(x)]^{j+1}/(j+1) \tag{14}$$

$$\psi_w(x) = -\int_0^{r_w(x)} \left[\frac{q_w{}^R(x) - 2\sigma\bar{T}_w{}^4/\bar{\rho}_\infty\bar{V}_\infty{}^3}{h_{\text{eff}}}\right] r^j dr \tag{15a}$$

for

$$q_w{}^R(x) > 2\sigma\bar{T}_w{}^4/\bar{\rho}_\infty\bar{V}_\infty{}^3, \quad \psi_w(x) = 0 \tag{15b}$$

otherwise.

Thus, the rate of mass flow in the blown layer is related to the net rate at which radiant energy is absorbed by the optically black surface through an effective heat of ablation. If the energy emitted by the surface is greater than that which is absorbed the blowing rate is set to zero.

In order to simplify specification of the divergence of the radiation flux vector, it is assumed that the radiation field is one-dimensional varying only with ψ. This familiar tangential slab approximation does not lead to serious errors as long as the shock and blown layers are thin compared to the local radius of curvature of the shock. The boundary conditions for the radiation field are 1) the boundary at $\psi = \psi_s(x)$ (that is, the bow shock) is transparent; 2) the freestream neither emits nor absorbs radiant energy; 3) the boundary at $\psi = \psi_w(x)$ (i.e., the body surface) is optically black at temperature $\bar{T}_w$; and 4) absorption in the shock layer of energy radiated from the body surface is negligible. In addition to the previous listed assumptions, a step-function (in frequency) model for the absorption coefficient similar to that presented in Ref. 1 is used herein. This model consists of eight steps in frequency which approximate the important contributions of the free-bound and free-free continua, atomic lines, and molecular band systems found in high-temperature air. A plot of this model together with a more detailed calculated spectrum is shown in Fig. 2. Formulas for each of the various steps are presented in Appendix A. A correlation formula which expresses the temperature in terms of the enthalpy and density is also used in the present calculations. This formula is presented in Appendix A.

With the foregoing assumptions the term on the right-hand side of Eq. (5) becomes

$$\frac{r_s{}^j(x)\rho^2\partial q_\psi{}^R}{(1+\chi)p\partial\psi} = -\frac{2\epsilon\rho^2}{(1+\chi)pu}\sum_{i=1}^{8}\kappa_i(x,\psi)\left[B_i(x,\psi) - \frac{k_p r_s}{j+1}\int_0^{\psi_s(x)}\frac{\kappa_i(x,\xi)}{u(x,\xi)}B_i(x,\xi)e^{-2k_p|\tau_i(x,\psi)-\tau_i(x,\xi)|}d\xi\right] = \epsilon\rho^2(x,\psi)Q(x,\psi) \tag{16}$$

Here the normalized optical depth is

$$\tau_i(x,\psi) = \frac{r_s(x)}{j+1}\int_{\psi/\psi_s}^{1}\frac{\kappa_i(x,\xi)}{u(x,\xi)}d\xi \tag{17}$$

Also $k_p = \bar{\rho}_\infty\bar{\kappa}_{p,st}\bar{R}_{st}$ is the Bouguer number or characteristic optical depth, and $\epsilon = (4\alpha\bar{T}_{st}{}^4/\bar{\rho}_\infty\bar{V}_\infty{}^3)k_p$ is the radiation cooling parameter. The substitute kernel approximation, wherein the exponential integral function $E_2(x)$ is replaced by the exponential function e^{-2x}, is also used in the derivation of Eq. (16).† The accuracy of this approximation is well documented.[3]

An iteration formula for the solution of $\rho(x,\psi)$ is obtained by formally integrating Eq. (5). The formula is

$$\rho^{(k+1)}(x,\psi) = \rho_i(\psi)\left[\frac{p(x,\psi)}{p_i{}^{(\psi)}}\right]^{(1-\chi)/(1+\chi)} \times \exp\left[\epsilon\int_{x_i(\psi)}^{x} Q^{(k)}(x,\psi)\rho^{(k)}(x,\psi)dx\right] \tag{18}$$

where the superscript (k) indicates the iteration number and the subscript i is s for the density in the shock layer and w for the density in the blown layer.

In order to eliminate the coupling between the blown layer and the shock layer, it is assumed that radiation from the blown layer has no effect on the shock layer. Chin[3] has shown that this assumption is valid in the stagnation region. Now the iteration formula [Eq. (18)] specialized to the shock and blown layers, respectively, becomes

$$\rho^{(k+1)}(x,\psi) = \rho_s(\psi)\left[\frac{p(x,\psi)}{p_s(\psi)}\right]^{(1-\chi)/(1+\chi)}\exp\left[\epsilon\int_{x_s(\psi)}^{x}Q^{s1(k)}(x,\psi)^{(k)}(x,\psi)dx\right] \tag{19}$$

$$\rho^{(k+1)}(x,\psi) = \rho_w(\psi)\left[\frac{p(x,\psi)}{p_w(\psi)}\right]^{(1-\chi)/(1+\chi)}\exp\left[\epsilon\int_{x_w(\psi)}^{x}Q^{b1(k)}(x,\psi)^{(k)}(x,\psi)dx\right] \tag{20}$$

where

$$Q_{s1}{}^{(k)}(x,\psi) = -\frac{2}{(1+\chi)pu^{(k)}}\sum_{i=1}^{8}\kappa_i{}^{(k)}(x,\psi)\left[B_i{}^{(k)}(x,\psi) - \frac{k_p r_s}{j+1}\int_0^{\psi_s(x)}\times \frac{\kappa_i{}^{(k)}(x,\xi)}{u^{(k)}(x,\xi)}B_i{}^{(k)}(x,\xi)e^{-2kx_p|\tau_i{}^{(k)}(x,\psi)-\tau_i{}^{(k)}(x,\xi)|}d\xi\right] \tag{21}$$

† This approximation is not necessary in the analysis and was used merely as a convenience.

and

$$Q_{b1}^{(k)}(x,\psi) = -\frac{2}{(1+\chi)pu^{(k)}}\sum_{i=1}^{8}\kappa_i^{(k)}(x,\psi)\left[B_i^{(k)}(x,\psi) - \frac{k_p r_s}{j+1}e^{-2k_p[\tau_i^{(k)}(x,\psi)-\tau_i^{(k)}(x,0)]}\cdot\int_0^{\psi_s(x)}\frac{\kappa_i(x,\xi)}{u(x,\xi)}\times B_i(x,\xi)e^{-2k_p|\tau_i(x,0)-\tau_i(x,\xi)|}d\xi - \frac{k_p r_s}{j+1}\int_{\psi_w(x)}^{0}\frac{\kappa_i^{(k)}(x,\xi)}{u^{(k)}(x,\xi)}\times B_i^{(k)}(x,\xi)e^{-2k_p|\tau_i^{(k)}(x,\psi)-\tau_i^{(k)}(x,\xi)|}d\xi\right] \quad (22)$$

It should be noted that the symbols for the optical and flow properties appearing in the first definite integral in Eq. (22) do not carry a superscript (k). That is because those values are given by the final shock-layer solution which is determined independently of and prior to the blown-layer solution. Solutions to both Eqs. (19) and (20) are achieved by iterating to a desired accuracy at successively larger values of ϵ until the desired value of ϵ is reached. The initial guess is obtained by setting ϵ to zero, and subsequent initial guesses are obtained by extrapolation from the previous results.

Because the solution of the blown layer affects the value of the radiant energy flux absorbed by the body surface, q_w^R, an additional iteration cycle on q_w^R is required to solve Eq. (20). Thus, several iteration cycles are required and were it not for the inherent simplicity of Maslen's method the calculations would require rather long computation times. The current version of the program takes about 3 min on a CDC 6600 for a grid including 21 stations across the shock layer and 20 stations along the shock with no blowing. When blowing is included and the grid is 16 × 11, in both the shock and blown layers, the computations take about 5 min. In both cases cited the final value of ϵ was about 0.16 and the step size in ϵ was 0.02. The computation time is strongly dependent on ϵ. Unequal increments in the stream-function coordinate ψ were used with the smaller increments located near the body surface. This provided adequate definition of the entropy layer without requiring an excessive number of grid points.

Results

This section will present a discussion of the nature of the flowfield of a radiating gas about a blunted cone, an evaluation of the capability of the present method to compute these flowfields, a discussion of the effects of cone angle and nose bluntness for a series of blunted cones, and finally, a preliminary look at the effects of an inviscid blown layer. The blunted conical bodies to be discussed were generated by assuming a shock shape given by the following formula:

$$z_s = Ar_s^2/(1 + Ar_s\tan\theta_s) \quad (23)$$

The quantity A serves as a bluntness parameter as it is inversely proportional to the radius of curvature of the shock at the stagnation streamline. Thus, bluntness decreases as A increases. The quantity θ_s represents the half-angle of the conical surface which is the asymptote of the shock for large values of r_s.

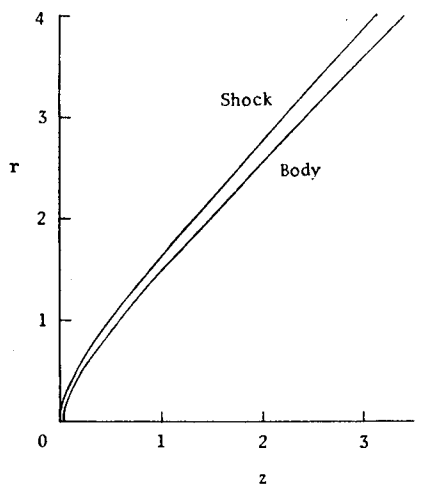

Fig. 3 Shock and body shape for 45° blunted cone; $\bar{V}_\infty$ = 12.2 km/sec, $\bar{\rho}/\bar{\rho}_0 = 2.24 \times 10^{-4}$, base radius = 1.22 m, A = 1.0, θ_s = 45.75°.

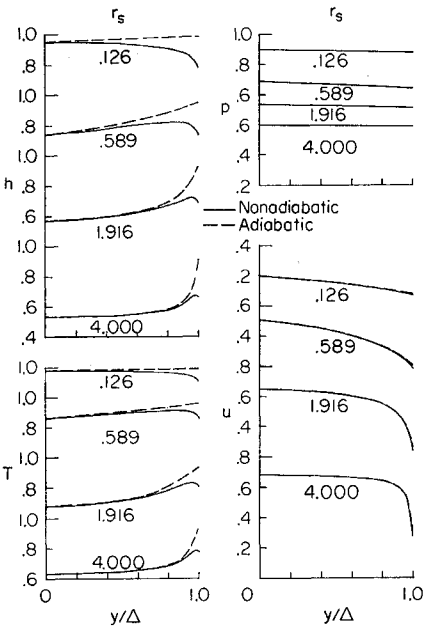

Fig. 4. Shock-layer profiles for 45° blunted cone; $\bar{V}_\infty$ = 12.2 km/sec, $\rho/\rho_0 = 2.24 \times 10^{-4}$, base radius = 1.22 m, A = 1.0, θ_s = 45.75°.

The shock shape and resultant body shape for A = 1.0 and θ_s = 45.75° are presented in Fig. 3. These values led to a nose radius of approximately 15.2 cm (0.5 ft) and a body cone angle of about 45°. The velocity was given as 12.2 km/sec (40,000 fps) and the freestream density as 2.24×10^{-4} of standard sea-level density (this corresponds to an altitude of about 200,000 ft, or 60.96 km). The effect of radiation on the standoff distance is small for this case, amounting to a reduction from the adiabatic value of less than 2% in the stagnation region and 0.2% at the downstream end of the conical portion of the body. Similar small effects were noted for all other cases studied. The largest reduction in standoff distance amounted to less than 9% at the downstream end of the conical portion of the bluntest 60° cone studied.

The enthalpy distributions across the shock layer at several body stations are presented in Fig. 4. The dashed curves show the results when radiation cooling effects are not taken into account. Near the axis of symmetry (see curve labeled r_s = 0.126) the enthalpy increases slowly across the shock layer from the shock to the body. Along the stagnation streamline (r = 0) the analysis of this paper leads to constant enthalpy across the shock layer. This result is consistent with the usual stagnation region approximations.[1] On the nearly conical portion of the body surface (r_s = 1.916 and 4.0) the enthalpy is almost constant except immediately adjacent to the body surface. A sharp pointed cone in a hypersonic stream would have a nearly constant enthalpy throughout the flowfield. That portion of the flow close to the body surface where the enthalpy increases sharply is known as the entropy layer. It contains those particles of gas which crossed the nearly normal portion of the bow shock

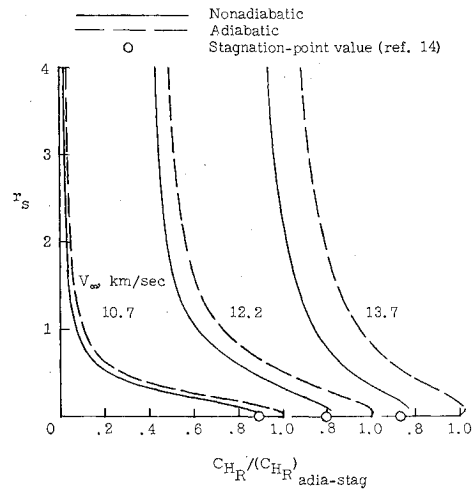

Fig. 5 Effect of freestream velocity on the radiative heating distribution for a 45° blunted cone; $\bar{\rho}/\bar{\rho}_0 = 2.24 \times 10^{-4}$, base radius = 1.22 m, $A = 1.0$, $\theta_s = 45.75°$.

in the vicinity of the stagnation streamline. Those particles were more severly compressed by the bow shock, and a larger amount of their initial kinetic energy was transformed to thermal energy with a subsequent larger increase in entropy. As the entropy layer flows along the body surface it becomes thinner because of the three-dimensional relieving effect. The pressure distribution across the shock layer (Fig. 4) is unaffected by the entropy layer while the temperature and tangential velocity show large gradients near the body surface. Because of the high temperatures in it the entropy layer can make an important contribution to the radiative heating of the body.

The nonadiabatic or cooling effects of radiation on the shock-layer distributions are shown by the solid curves in Fig. 4. For the two radial stations closest to the stagnation streamline, the results are similar to results obtained with stagnation region analyses.[1,2] However, if the step size in r were reduced so that results were obtained for r close to zero, the shock-layer distributions, while showing a general qualitative behavior similar to those obtained with stagnation region analyses, would not be in quantitative agreement. In fact, differences as large as 10 or 20% in enthalpy near the body would be found for the conditions of this example. These large differences are a result of large differences in particle residence times in the stagnation region for the two different types of analyses. As a result of this difficulty, the calculations for the first one or two body stations closest to the stagnation streamline are considered to be invalid and will not be presented. The number of body stations in error seems to be nearly independent of increment size in r as long as the increment size is not much smaller than the standoff distance. The inaccuracy of the shock-layer distributions in the vicinity of the stagnation point lead to errors in the calculation of the standoff distance. These errors were estimated to be less than about 1% for the cases treated herein.

The effect of radiation cooling on the properties of the entropy layer at the stations $r_s = 1.916$ and 4.0 is quite significant. The enthalpy and temperature are considerably reduced from the adiabatic levels. Most of this reduction results from energy losses in the stagnation region. Of course, the presence of the cold body surface and the relatively slow motion and, hence, long residence times of gas particles in the entropy layer does lead to some further cooling. The relative importance of these two components of the cooling effect depends on the nose radius and afterbody cone angle. For the present case, cooling is not sufficient to reduce the enthalpy and temperature to values as low as those outside the entropy layer (where cooling is negligible). Thus, the maximum values of these quantities are still located in the entropy layer although they are no longer immediately adjacent to the body surface. The reduced temperature in the entropy layer has important implications for the computation of both radiative and convective heating.

The radiative heat-transfer coefficient C_{HR} normalized with respect to its adiabatic stagnation-point value is presented in Fig. 5 as a function of the body radial station for three different values of freestream velocity. The dashed and solid lines represent results when radiation cooling is neglected and properly taken into account, respectively. The nonadiabatic stagnation-point values represented by the open circle symbols were determined by applying cooling factor correlations[14] to the adiabatic stagnation values obtained by extrapolating the present adiabatic values to $r = 0$. The nonadiabatic results obtained by the present method tend toward somewhat higher stagnation-point values than those predicted with the cooling factor correlations, because of the inadequacy of the present approach in the vicinity of the stagnation region. The mass of the air which passed through the stagnation region becomes a rapidly diminishing fraction of the total mass in the shock layer with increasing r, and, in fact, is only a small fraction of the mass in the entropy layer for values of r large compared to the standoff distance. Consequently, it is expected that the errors introduced in the stagnation region will not influence the downstream results to any significant degree.

The radiative heating distribution for a sharp 45° half-angle cone would be monotonically increasing with r as a result of the increasing standoff distance. This is not the case here indicating that the distributions are determined primarily by the entropy layer which becomes thinner and cooler as r increases. Even when cooling is taken into account the entropy layer is still the dominant contributor to the radiative heating. It can also be inferred from this figure that much of the temperature reduction in the entropy layer was caused by cooling in the stagnation region, as the heating rate to the body surface (i.e., energy lost from the gas by radiation) is much larger in the stagnation region than elsewhere.

It should also be noted that the adiabatic and nonadiabatic radiative heating distributions for a given freestream velocity are not similar. This is not in agreement with results of other works[9,10] in which the analyses are restricted to the subsonic portion of the shock layer about a sphere.‡ In addition, it is shown that neither the adiabatic nor the nonadiabatic distributions are similar for different freestream velocities. This result is in contrast to the result for laminar convective heating distributions which are approximately similar for different hypersonic freestream velocities.

The effect of bluntness on the heat-transfer coefficient distribution along the body surface for cones of approximately 60° half-angle is shown in Fig. 6. The freestream velocity, density, and base radius (the base is considered to be at $r = 4.0$) were 12.2 km/sec, 2.24×10^{-4} times standard sea-level density, and 1.22 m for all cases. The bluntness parameter A varied from $\frac{1}{4}$ to ∞ (sharp cone). The adiabatic heat-transfer coefficient (dashed lines) is larger at all body stations for greater bluntness (smaller A). This is caused by increases in standoff distance, entropy layer thickness, and local shock angle (because of the shock shape equation used here, the transition region between the blunt nose and the asymptotic cone can be quite extensive) with increasing bluntness. When radiation cooling is properly accounted

‡ One of the reference works[9] is a viscous analysis. However, it was shown that the effect of the boundary layer on the radiative heating distribution was small. It will be shown later in this paper that the adiabatic and nonadiabatic radiative heating distributions are similar in the subsonic flow region for a paraboloidal shock.

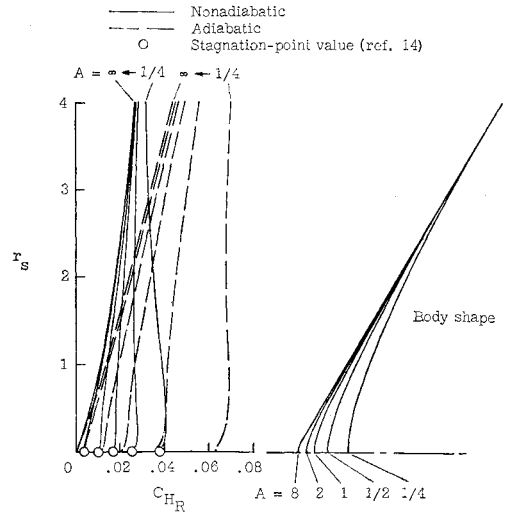

Fig. 6 Radiative heating distributions for a series of 60° blunted cones; $\bar{V}_\infty$ = 12.2 km/sec, $\bar{\rho}/\bar{\rho}_0 = 2.24 \times 10^{-4}$, base radius = 1.22 m.

for (solid lines) the differences due to bluntness are in the same direction but are considerably reduced in magnitude. Furthermore, the smaller bluntness cone (larger A) heating distributions quickly approach the sharp cone limit. This is to be expected because of the effect of radiation cooling on the entropy layer. The significant difference between the adiabatic and nonadiabatic heating distributions for the sharp cone ($A = \infty$) indicate that cooling is important outside of the entropy layer on the conical afterbody and that the local standoff distance (which increases with both r and $1/A$) and the local shock angle are at least as important as the entropy layer in determining the radiative heating distribution. In fact, the effect of the entropy layer on the nonadiabatic results is quite small because the entropy layer temperatures are everywhere less than the temperatures outside the entropy layer. As was the case for the 45° blunted cone discussed previously, the adiabatic and nonadiabatic heating distributions are not similar for any of the 60° blunted cones studied.

The effect of bluntness on the radiative heating-rate distributions along the surfaces of three-45° blunted cones is shown in Fig. 7. The freestream conditions and the cone base radii are the same as for the previous figure. Because of the large variation of C_{HR} with radial station, a logarithmic scale has been used. The difference between the adiabatic and nonadiabatic results for the sharp cone ($A = \infty$) are indistinguishable on this plot, indicating that cooling will only be important in the stagnation regions and entropy layers of the two blunted cones. The results for the sharper of the two blunted cones ($A = 8$) indicate that most of the cooling occurs on the conical afterbody downstream of the stagnation point. It is interesting to note that even though the radiative heating rate is not large, the percentage change due to cooling is quite large. This occurs because the adiabatic heating rate is dominated by the very thin high-temperature entropy layer. While this layer may not contain much energy compared to the rest of the flowfield, it is in a form (high temperature) favorable to rapid radiative cooling. The results for the bluntest cone ($A = 1$) have been discussed previously (with reference to Fig. 5). Suffice it to say here that a significant amount of cooling does occur in the stagnation region and that the entropy layer does not lose its influence on the heating rate even toward the end of the conical afterbody. This, of course, is a result of increased entropy layer thickness with increased bluntness and a slower transition of the body geometry from the blunt nose to the conical afterbody.

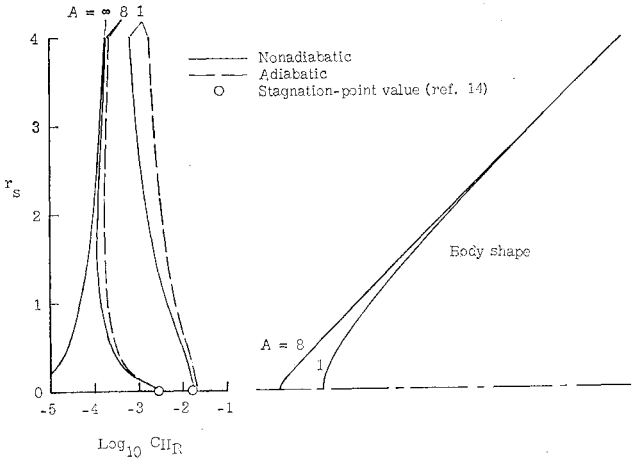

Fig. 7 Radiative heating distributions for a series of 45° blunted cones; $\bar{V}_\infty$ = 12.2 km/sec, $\bar{\rho}/\bar{\rho}_0 = 2.24 \times 10^{-4}$, base radius = 1.22 m.

The radiative heat-transfer distributions for three cones of approximately 30° half-angle and different amounts of bluntness are shown in Fig. 8. Here the freestream velocity is 15.2 km/sec while the freestream density and the cone base radii are the same as in the previous examples. Again a logarithmic scale has been used for C_{HR}. The adiabatic and nonadiabatic results for the sharp cone ($A = \infty$) are indistinguishable so that cooling must be restricted to the stagnation region and entropy layers of the two blunted cones. The sharper of the two blunted cones experiences negligible cooling in the stagnation region. However, cooling in the entropy layer on the conical afterbody reduces the already small heating rate by almost a factor of three. The results for the bluntest cone ($A = 2$) show some cooling in the stagnation region (the nonadiabatic heating rate is about 20% less than the adiabatic rate) and a considerable amount of cooling in the entropy layer downstream.

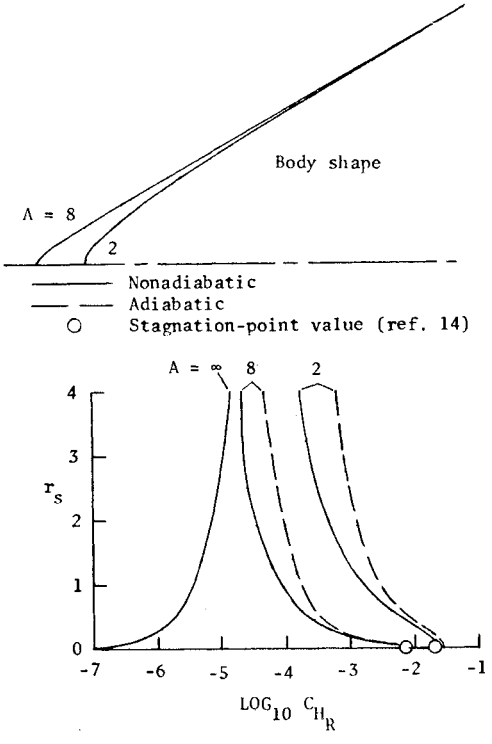

Fig. 8 Radiative heating distributions for a series of 30° blunted cones; $\bar{V}_\infty$ = 15.2 km/sec, $\bar{\rho}/\bar{\rho}_0 = 2.24 \times 10^{-4}$, base radius = 1.22 m.

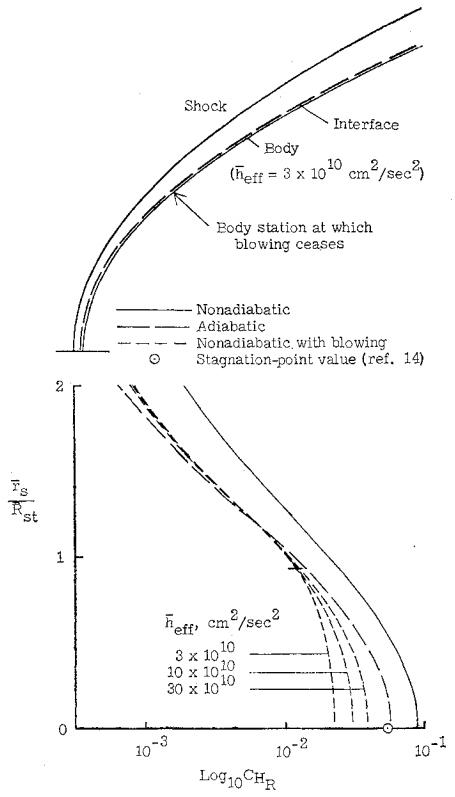

Fig. 9 Blown-layer thickness and radiative heating distributions for a paraboloidal shock; $\bar{V}_\infty$ = 15.2 km/sec, $\bar{\rho}/\bar{\rho}_0$ = 2.24 × 10^{-4}, stagnation-region shock radius = 0.305 m, $\bar{T}_w$ = 3300°K.

While the effects of cooling on the conical afterbody radiative heating rates appear to be dramatic, it should be pointed out that the magnitude of these radiative heating rates are quite small for the 30° and 45° half-angle cones and would not make any significant contribution to the total (radiative plus convective) heat transfer. However, the cooling of the entropy layer due to radiation may have an important effect on the calculation of convective heat-transfer rates on the conical afterbody.

Some preliminary results which include the presence of an inviscid blown layer have been obtained and will be discussed here. The shock shape used in the calculations was a parabola of revolution given by the formula

$$\bar{z}_s = \bar{r}_s^2/2\bar{R}_{st} \qquad (24)$$

The freestream velocity was 15.2 km/sec, the density 2.24 × 10^{-4} of standard sea-level density, and the shock radius of curvature at the stagnation streamline was 0.305 m. A surface temperature of 3300°K and effective heats of ablation of 3 × 10^{10}, 10 × 10^{10}, and 30 × 10^{10} cm^2/sec^2 were used to specify the rate of mass loss from the surface according to Eq. (15). The resulting body shape for the smallest effective heat of ablation and the largest blown-layer thickness is shown in Fig. 9. (The blown-layer thickness varies inversely with the effective heat of ablation.)

The heating distributions for the various bodies obtained are also shown in Fig. 9. The effect of radiation cooling is seen to be quite important as the nonadiabatic (without blowing) heating rates are only about 64% of the adiabatic (without blowing) rates in the stagnation region and 33% at the last body station ($\bar{r}_s/\bar{R}_{st}$ = 2.0). The percent reduction is nearly independent of the radial station for the portion of the body upstream of the sonic point ($\bar{r}_s/\bar{R}_{st} \approx 0.667$). This agrees with previous works[9,10] which studied the subsonic portion of hemispherical bodies. Blowing from the body surface occurred upstream of body station $\bar{r}_s/\bar{R}_{st}$ = 0.933. The thermodynamic and optical properties of the blown layer were assumed to be the same as for the shock layer; that is, like air. In the stagnation region blowing is quite effective in reducing the radiative heating to the body surface. However downstream of the stagnation region, where the radiative heat flux from the hot shock layer decreases, re-emission from the blown layer becomes increasingly important compared with absorption. Thus the effectiveness of the blown layer decreases and finally becomes negative, so that the presence of the blown layer actually increases the radiative heating of the body surface downstream of the body station where blowing ceases.

The reduction in heating rate due to blowing depends on the blown-layer thickness and, hence, the effective heat of ablation. The reduction ranges from 57% at r = 0.267 for the smallest effective heat of ablation (3 × 10^{10} cm^2/sec^2) to 30% at r = 0.267 for the largest effective heat of ablation (30 × 10^{10} cm^2/sec^2). Perhaps of even greater importance is the reduction in mass loss from the surface when absorption in the blown layer is taken into account. This reduction ranges from 77% for the smallest effective heat of ablation to 40% for the largest, also at r = 0.267. The mass loss from the surface is seen to be quite sensitive to the heating rate. This is because the rate at which energy is radiated away from the surface is a considerable percent (about 26% at r = 0.267) of the incoming heating rate for no blowing under the conditions considered here.

The enthalpy distribution across the shock and blown layer at r = 0.267 is shown in Fig. 10 for the two extreme values of the effective heat of ablation. In both cases there is a large enthalpy gradient in the blown layer adjacent to the interface with the shock layer. The higher enthalpy in this region is a result of the absorption of energy emitted by the hot shock layer. The small extent of the large gradient region indicates that the energy absorbed therein is primarily that energy emitted in the vacuum ultraviolet portion of the spectrum for which the blown layer is optically thick. The enthalpy in the remainder of the blown layer, for the smallest effective heat of ablation, is slightly higher than the enthalpy which could be computed for a transparent blown layer, and most of the energy absorbed there is in the visible and infrared portions of the spectrum for which the blown layer is optically thin. It is the absorption of the visible and infrared radiation which is primarily responsible for the greater reduction in heating rate achieved as the effective heat of ablation is decreased.

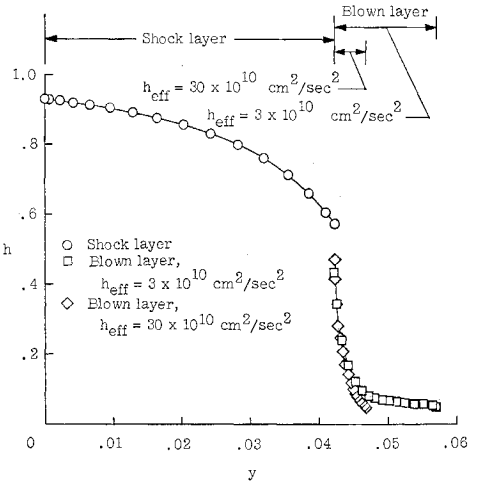

Fig. 10 Shock- and blown-layer enthalpy profiles at $\bar{r}_s/\bar{R}_{st}$ = 0.267 for a paraboloidal shock; $\bar{V}_\infty$ = 15.2 km/sec, $\bar{\rho}/\bar{\rho}_0$ = 2.24 × 10^{-4}, stagnation-region shock radius = 0.305m, $\bar{T}_w$ = 3300°K.

The distribution of the tangential velocity across the shock and blown layers for $r = 0.267$ is shown in Fig. 11 for the two extreme values of the effective heat of ablation. The most noticeable aspect of these results is the large change in velocity in the blown layer adjacent to the interface. The velocity immediately adjacent to the interface is almost three times what it would be if the blown layer were perfectly transparent. This change in velocity due to absorption is in the same direction as the change that would result from including viscosity, and although the velocity is not continuous through the interface it does have some of the character of a free shear layer associated with massive blowing. Thus the penalty incurred through use of the inviscid approximation seems not to be quite so severe when radiative transport is taken into account.

Concluding Remarks

The purpose of this paper was to study the effects of radiation on the flow about smooth symmetric bodies downstream of the stagnation region. A realistic nongray absorption coefficient model was utilized and the effects of radiation cooling were taken into account. It was shown, under the conditions considered herein (freestream velocity from 10.7 to 15.2 km/sec and altitude equal to 60.96 km), that the effect of radiation on the shock standoff distance was small, leading to a slight reduction. However, the effect of radiation on the properties of the entropy layer could be very significant, in some cases changing the entropy layer from a region of relative high temperature to a region of relative low temperature. Such effects have important implications on the determination of both the radiative and convective heating of the body surface. It was also shown that the radiative heating distribution was strongly influenced by the local shock angle (which largely determines the temperature environment outside the entropy layer (the shock standoff distance) a function of nose bluntness), and the nature of the entropy layer. It was seen that radiation cooling can lead to a larger reduction in heating (from the adiabatic value) on the conical surface than at the stagnation point as a result of the large influence of the entropy layer. The adiabatic and nonadiabatic (radiation cooling properly accounted for) radiative heating distributions were seen to be dissimilar for all blunted cones studies. This result is in contradiction to earlier results[9,10] and the present paper for the flow in the subsonic region about nearly spherical bodies. The radiative heating rate distributions for different freestream velocities for a given blunted cone were also shown to be dissimilar. Finally, it was shown that the presence of a blown layer leads to a reduction in radiative heating rate in addition to that caused by radiation cooling. The amount of this reduction increased with blowing rate for a given gas composition and surface condition.

Appendix: Approximate Thermodynamic and Optical Properties for High-Temperature Air

The absorption coefficient model used to represent the optical properties of high-temperature air is shown in Fig. 2. It consists of eight steps in frequency. Actually one of these steps (which accounts for atomic line radiation in the ultraviolet portion of the spectrum) might better be labeled an effective step as it is an approximate mathematical representation of a series of tall, thin steps of equal height, width, and spacing. For a discussion of this "picket fence" model see Ref. 1. Formulas for the heights of each of the eight steps are listed below:

$$\bar{\kappa}_1 = 1.1 \times 10^{-17} \frac{(\mathrm{N})}{\bar{\rho}} + 2.0 \times 10^{-17} \frac{(\mathrm{O}_2)}{\bar{\rho}} + 4.0 \times 10^{-16} \frac{(\mathrm{N}_2)}{\bar{\rho}} + \bar{\kappa}_2 \quad \text{(A1)}$$

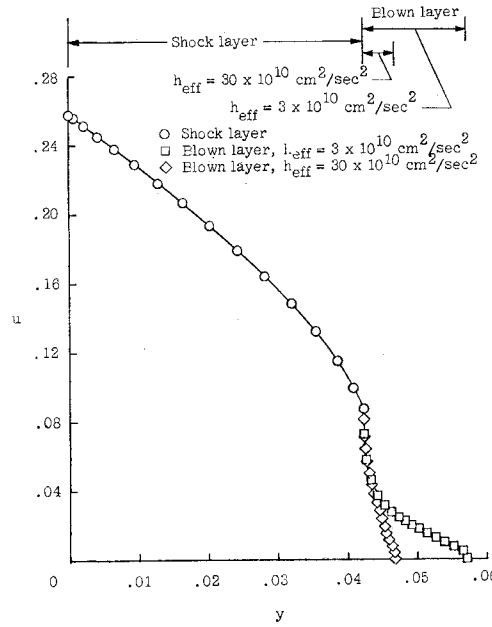

Fig. 11 Shock and blown layer tangential velocity profiles at $\bar{r}_s/\bar{R}_{st} = 0.267$ for a paraboloidal shock; $\bar{V}_\infty = 15.2$ km/sec, $\bar{\rho}/\bar{\rho}_0 = 2.24 \times 10^{-4}$, stagnation-region shock radius = 0.305 m, $\bar{T}_w = 3300$°K.

$$\bar{\kappa}_2 = 5.1 \times 10^{-18} [(\mathrm{O}_2) + (\mathrm{N}_2) + (\mathrm{O})]/\bar{\rho} + \bar{\kappa}_3 \quad \text{(A2)}$$

$$\bar{\kappa}_3 = 2.0 \times 10^{-18} \frac{(\mathrm{O}_2) + (\mathrm{N}_2)}{\bar{\rho}} + 2.1 \times 10^{-17} \frac{(\mathrm{N})}{\bar{\rho}} e^{-0.165/\tilde{T}} + \bar{\kappa}_4 \quad \text{(A3)}$$

$$\bar{\kappa}_4 = 5.0 \times 10^{-19} \frac{(\mathrm{O}_2)}{\bar{\rho}} + 5.0 \times 10^{-20} \frac{(\mathrm{N}_2)}{\bar{\rho}} + 1.7 \times 10^{-17} \frac{(\mathrm{N})}{\bar{\rho}} e^{-0.246/\tilde{T}} \quad \text{(A4)}$$

$$\bar{\kappa}_5 = 7.7 \times 10^{-17} \frac{(\mathrm{O}_2) + (\mathrm{N}_2)}{\bar{\rho}} e^{-0.490/\tilde{T}} + 2.6 \times 10^{-17} \frac{(\mathrm{O}) + (\mathrm{N})}{\bar{\rho}} e^{-0.723/\tilde{T}} \quad \text{(A5)}$$

$$\bar{\kappa}_6 = 2.0 \times 10^{-18} \frac{(\mathrm{O}_2)}{\bar{\rho}} + 1.5 \times 10^{-17} \frac{(\mathrm{O}) + (\mathrm{N})}{\bar{\rho}} e^{-0.379/\tilde{T}} + \bar{\kappa}_5 \quad \text{(A6)}$$

$$\bar{\kappa}_7 = 3.0 \times 10^3 [(\mathrm{O}) + (\mathrm{N})/\bar{\rho}(e^-)] e^{-0.489/\tilde{T}} + \bar{\kappa}_6 \quad \text{(A7)}$$

$$\bar{\kappa}_8 = 3.2 \times 10^{-17} [(\mathrm{O}) + (\mathrm{N})/\bar{\rho}] e^{-0.631/\tilde{T}} + \bar{\kappa}_5 \quad \text{(A8)}$$

Here

$$\tilde{T} = \bar{T}(°\mathrm{K})/168{,}800 \quad \text{(A9)}$$

$$\tilde{\nu} = 852/\lambda(\text{Å}) \quad \text{(A10)}$$

The temperature 168,800°K and the wavelength 852 Å correspond to the ionization potential of the ground state of the neutral nitrogen atom. The quantities (A) represent the concentration in particles/cm^3 of the species A. These species concentrations are calculated in the program with a simplified statistical mechanical model of air similar to that developed by Hansen.[15]

The formulas (A1–A4) were obtained by curve fitting the tabulated values presented in Ref. 1. Formulas (A6) and (A7) were obtained by curve fitting tabulated values[1] for steps seven and eight and multiplying the result by 20. This correction was applied because the f numbers on which the values of the reference are based were shown by Wilson and Nicolet[16] to be too small on the average by a factor of about 20. Formulas (A5) and (A8) were obtained by curve fitting tabulated data[4] for the "visible continuum" and "IR lines," respectively.

Values of the integrated Planck function for use in the frequency intervals previously listed were obtained with the formula

$$(\pi/\sigma\bar{T}^4)\int_{\tilde{\nu}/\tilde{T}}^{\infty}\bar{B}_{\tilde{\nu}}d(\tilde{\nu}/\tilde{T}) \approx \frac{15}{\pi^4}\left\{e^{-\tilde{\nu}/\tilde{T}}\left[6+6\left(\frac{\tilde{\nu}}{\tilde{T}}\right)+3\left(\frac{\tilde{\nu}}{\tilde{T}}\right)^2+\left(\frac{\tilde{\nu}}{\tilde{T}}\right)^3\right]\times \frac{1}{2}e^{-2\tilde{\nu}/\tilde{T}}\left[\frac{3}{4}+\frac{3}{2}\left(\frac{\tilde{\nu}}{\tilde{T}}\right)+\frac{3}{2}\left(\frac{\tilde{\nu}}{\tilde{T}}\right)^2+\left(\frac{\tilde{\nu}}{\tilde{T}}\right)^3\right]\right\} \quad (A11)$$

This formula gives 1% or better accuracy for $\tilde{\nu}/\tilde{T} \geq 1.75$ which always holds for the calculations of this paper. Now with (A11),

$$B_1 = (\bar{T}/\bar{T}_{st})^4(\pi/\sigma\bar{T}^4)\int_{1.0/\tilde{T}}^{\infty}\bar{B}_{\tilde{\nu}}d(\tilde{\nu}/\tilde{T}) \quad (A12)$$

$$B_2 = (\bar{T}/\bar{T}_{st})^4(\pi/\sigma\bar{T}^4)\int_{0.935/\tilde{T}}^{\infty}\bar{B}_{\tilde{\nu}}d(\tilde{\nu}/\tilde{T}) - B_1 \quad (A13)$$

$$B_3 = (\bar{T}/\bar{T}_{st})^4(\pi/\sigma\bar{T}^4)\int_{0.835/\tilde{T}}^{\infty}\bar{B}_{\tilde{\nu}}d(\tilde{\nu}/\tilde{T}) - B_2 - B_1 \quad (A14)$$

$$B_4 = (\bar{T}/\bar{T}_{st})^4(\pi/\sigma\bar{T}^4)\int_{0.754/\tilde{T}}^{\infty}\bar{B}_{\tilde{\nu}}d(\tilde{\nu}/\tilde{T}) - B_3 - B_2 - B_1 \quad (A15)$$

$$B_5 = (\bar{T}/\bar{T}_{st})^4 - B_8 - B_6 - B_4 - B_3 - B_2 - B_1 \quad (A16)$$

$$B_6 = (\bar{T}/\bar{T}_{st})^4(\pi/\sigma\bar{T}^4)\int_{0.473/\tilde{T}}^{\infty}\bar{B}_{\tilde{\nu}}d(\tilde{\nu}/\tilde{T}) - B_4 - B_3 - B_2 - B_1 \quad (A17)$$

$$B_7 = 2.4 \times 10^{-21}(e^{-})B_6\exp(0.162/\tilde{T}) \quad (A18)$$

$$B_8 = (\bar{T}/\bar{T}_{st})^4\left[1-(\pi/\sigma\bar{T}^4)\int_{0.213/\tilde{T}}^{\infty}\bar{B}_{\tilde{\nu}}d(\tilde{\nu}/\tilde{T})\right] \quad (A19)$$

Here the quantity B_7 represents the effective width to space ratio of the tall, thin steps in the picket fence model.

In order to evaluate the quantities $\bar{\kappa}_i$ and B_i it was necessary to first compute the temperature in terms of the enthalpy and density. The following correlation formulas were used for this purpose:

$$\bar{h}^*/R\bar{T}_0 = 1.02 \times 10^3(\bar{\rho}/\bar{\rho}_0)^{0.0526} \quad (A20)$$

If $\bar{h}^*/R\bar{T}_0 > \bar{h}/R\bar{T}_0$, then

$$\bar{T} = 10^4 f_1(\zeta_1)(\bar{\rho}/\bar{\rho}_0)^{0.0689} \quad (A21)$$

where

$$f_1(\zeta_1) = 2.68270 - 6.70367\zeta_1 + 12.6342\zeta_1^2 - 10.2562\zeta_1^3 + 4.17342\zeta_1^4 - 0.81420\zeta_1^5 + 0.0605669\zeta_1^6 \quad (A22)$$

and

$$\zeta_1 = 10^{-3}(\bar{h}/R\bar{T}_0)(\bar{\rho}/\bar{\rho}_0)^{-0.0177} \quad (A23)$$

If $\bar{h}^*/R\bar{T}_0 \leq \bar{h}/R\bar{T}_0$, then

$$\bar{T} = 10^3 f_2(\zeta_2)\left(\frac{\bar{\rho}}{\bar{\rho}_0}\right)^{0.0453} \quad (A24)$$

where

$$f_2(\zeta_2) = -0.0146891 + 5.83066\zeta_2 - 0.542786\zeta_2^2 - 0.629781\zeta_2^3 + 0.224193\zeta_2^4 - 0.0269783\zeta_2^5 + 0.00111033\zeta_2^6 \quad (A25)$$

and

$$\zeta_2 = 0.01(\bar{h}/R\bar{T}_0) \quad (A26)$$

Here

$$\bar{\rho}_0 = 1.288 \times 10^{-3}\text{g/cm}^3, \quad R\bar{T}_0 = 7.874 \times 10^8\text{cm}^2/\text{sec}^2 \quad (A27)$$

These formulas were obtained by curve fitting the tabulated data of Browne.[17] The maximum difference in temperature between the present correlation formulas and the tabulated data was about 250°K for the range of conditions considered in this paper.

References

[1] Olstad, W. B., "Blunt-Body Stagnation-Region Flow with Nongray Radiation Heat Transfer—A Singular Perturbation Solution," TR R-295, 1968, NASA.

[2] Callis, L. B., "Solutions of Blunt-Body Stagnation-Region Flows with Nongray Emission and Absorption of Radiation by a Time-Asymptotic Technique," TR R-299, 1969, NASA.

[3] Chin, J. H., "Radiation Transport for Stagnation Flows Including Effects of Lines and Ablation Layer," *AIAA Journal*, Vol. 7, No. 7, July 1969, pp. 1310–1318.

[4] Page, W. A. et al., "Radiative Transport in Inviscid Nonadiabatic Stagnation-Region Shock Layers," AIAA Paper 68-784, Los Angeles, Calif., 1968.

[5] Hoshizaki, H. and Lasher, L. E., "Convective and Radiative Heat Transfer to an Ablating Body," AIAA Paper 67-327, New Orleans, La., 1967.

[6] Coleman, W. D. et al., "A Study of the Effects of Environmental and Ablator Performance Uncertainties on Heat Shielding Requirements for Blunt and Slender Hyperbolic-Entry Vehicles," AIAA Paper 68-154, New York, 1968.

[7] Cheng, P. and Vincenti, W. G., "Inviscid Radiating Flow over a Blunt Body," *Journal of Fluid Mechanics*, Vol. 27, No. 4, 1967, pp. 625–646.

[8] Wang, K., "Radiating and Absorbing Steady Flow over Symmetric Bodies," *Journal of Quantitative Spectroscopy and Radiative Transfer*, Vol. 8, No. 1, Jan. 1968, pp. 119–144.

[9] Hoshizaki, H. and Wilson, K. H., "Convective and Radiative Heat Transfer During Superorbital Entry," *AIAA Journal*, Vol. 5, No. 1, Jan. 1967, pp. 25–35.

[10] Suttles, J. T., "A Method of Integral Relations Solutions to the Nonadiabatic Radiation Problem for an Inviscid Blunt-Body Flow Field," M.S. thesis, March 1968, Virginia Polytechnic Institute, Blacksburg, Va.

[11] Burns, R. K. and Oliver, C. C., "Downstream Radiation Flux to Blunt Entry Vehicles," *AIAA Journal*, Vol. 6, No. 12, Dec. 1968, pp. 2452, 2453.

[12] Maslen, S. H., "Inviscid Hypersonic Flow Past Smooth Symmetric Bodies," *AIAA Journal*, Vol. 2, No. 6, June 1964, pp. 1055–1061.

[13] Cole, J. D. and Aroesty, J., "The Blowhard Problem-Inviscid Flows with Surface Injection," *International Journal of Heat and Mass Transfer*, Vol. 11, No. 7, July 1968, pp. 1167–1183.

[14] Olstad, W. B., "Correlations for Stagnation-Point Radiative Heat Transfer," *AIAA Journal*, Vol. 7, No. 1, Jan. 1969, pp. 170–172.

[15] Hansen, C. F., "Approximations for the Thermodynamic and Transport Properties of High Temperature Air," TR R-50, 1959, NASA.

[16] Wilson, K. H. and Nicolet, W. E., "Spectral Absorption Coefficients of Carbon, Nitrogen, and Oxygen Atoms, *Journal of Quantitative Spectroscopy and Radiative Transfer*, Vol. 7, No. 6, Nov.-Dec. 1967, pp. 891–941.

[17] Browne, W. G., "Thermodynamic Properties of the Earth's Atmosphere," Radiation and Space Physics TM 2, Nov. 1962, Missile and Space Division, General Electric Co., Phila., Pa.